

Comparing distinct dissociation pathways of $C_2H_2^{2+}$ under laser and electron impact

Xiangjie Chen(陈祥杰), Jianting Lei(雷建廷), Chenyu Tao(陶琛玉), Shuncheng Yan(闫顺成), Yongzhe Ma(马永哲), Fenghao Sun(孙烽豪), Qincao Liu(刘情操), and Shaofeng Zhang(张少锋)
Citation: Chin. Phys. B, 2026, 35 (**4**): 043202. DOI: 10.1088/1674-1056/ae311d
http://cpb.iphy.ac.cn; http://iopscience.iop.org/cpb

What follows is a list of articles you may be interested in

Angular momentum distribution of atomic hydrogen in excited states under ultra-short laser field

Zhaoyan Zhou(周兆妍), Dongwen Zhang(张栋文), and Zengxiu Zhao(赵增秀)
Chin. Phys. B, 2026, 35 (**3**): 033201. DOI: 10.1088/1674-1056/adfdc6

Semiclassical Coulomb-scattering model for strong-field tunneling ionization

Qing Zhao(赵晴), Yigen Peng(彭易根), Jiayin Che(车佳殷), Chao Chen(陈超), Shang Wang(王赏), Guoguo Xin(辛国国), and Yanjun Chen(陈彦军)
Chin. Phys. B, 2025, 34 (**9**): 093201. DOI: 10.1088/1674-1056/ade06e

Theory and applications of attosecond transient absorption spectroscopy: From atoms to solids

Ennan Cui and Difa Ye(叶地发)
Chin. Phys. B, 2025, 34 (**7**): 073201. DOI: 10.1088/1674-1056/add1ba

Theoretical investigations of population trapping phenomena in atomic four-color, three-step photoionization scheme

Xiao-Yong Lu(卢肖勇) and Ya-Peng Sun(孙亚鹏)
Chin. Phys. B, 2024, 33 (**3**): 033202. DOI: 10.1088/1674-1056/ad10fc

Nonadiabatic molecular dynamics simulation of ${{\rm{C}}}_{2}{{\rm{H}}}_{2}^{2+}$ in a strong laser field

Ji-Gen Chen(陈基根), Gang-Tai Zhang(张刚台), Ting-Ting Bai(白婷婷), Jun Wang(王俊), Ping-Ping Chen(陈平平), Wei-Wei Yu(于伟威)§, and Xi Zhao(赵曦)¶
Chin. Phys. B, 2020, 29 (**11**): 113202. DOI: 10.1088/1674-1056/abb3de

---

SPECIAL TOPIC — Ultrafast physics in atomic, molecular and optical systems

Comparing distinct dissociation pathways of $C_2H_2^{2+}$ under laser and electron impact

Xiangjie Chen(陈祥杰)[1], Jianting Lei(雷建廷)[1,2,†], Chenyu Tao(陶琛玉)[2], Shuncheng Yan(闫顺成)[2], Yongzhe Ma(马永哲)[1], Fenghao Sun(孙烽豪)[1], Qingcao Liu(刘情操)[1,‡], and Shaofeng Zhang(张少锋)[2,3,4,§]

[1] *College of Science, Harbin Institute of Technology, Weihai* 264209, *China*
[2] *Institute of Modern Physics, Chinese Academy of Sciences, Lanzhou* 730000, *China*
[3] *University of Chinese Academy of Sciences, Beijing* 100049, *China*
[4] *State Key Laboratory of Heavy Ion Science and Technology, Lanzhou* 730000, *China*

(Received 23 October 2025; revised manuscript received 21 December 2025; accepted manuscript online 25 December 2025)

We report a comparative study of the dissociation dynamics of ethyne (C_2H_2) molecules and clusters under a strong laser field (9×10^{13} W/cm^2) and 1 keV electron impact. Using coincidence momentum imaging, we identify several two-body dissociation channels of $C_2H_2^{2+}$, including $C_2H^+ + H^+$, $CH_2^+ + C^+$, symmetric breakup into $CH^+ + CH^+$, as well as dimer dissociation channels such as $C_2H_2^+ + C_2H_2^+$ and $C_2H_2^{2+} + C_2H_2^+$. By analyzing the kinetic energy release (KER) and branching ratios of the dominant fragmentation pathways, we demonstrate that double ionization under a strong laser field preferentially leads to dissociation on the singlet ground-state surface ($^1\Delta_g$), whereas electron impact favors the triplet ground state ($^3\Sigma_g^-$). This contrast is attributed to different ionization mechanisms: electron impact follows a propensity rule favoring the lower-energy triplet, while strong-field ionization aligned with the π orbitals promotes singlet formation due to the Pauli exclusion principle. Our findings provide clear evidence of excitation-condition-dependent dissociation pathways in acetylene dications.

Keywords: coincidence measurement, kinetic energy release (KER), Coulomb explosion, dissociation dynamics

PACS: 32.80.–t, 32.10.–f, 32.80.Rm, 33.80.–b

DOI: 10.1088/1674-1056/ae311d **CSTR:** 32038.14.CPB.ae311d

1. Introduction

Hydrocarbons are fundamental building blocks in the formation of polycyclic aromatic hydrocarbons (PAHs) in interstellar environments.[1–5] Understanding their reaction pathways is crucial for deciphering the origin and evolution of organic molecules in the universe. Moreover, the properties of organic molecules are intrinsically linked to the origin and development of life, making the study of hydrocarbons pivotal for unraveling the formation processes of biological macromolecules associated with life's origin.[6–8] Among hydrocarbons, C_2H_2 is one of the simplest yet thermodynamically stable representatives. Consequently, the C_2H_2 molecule and the unique characteristics of its ionic species have been the subject of extensive experimental and theoretical investigations.[9–11] C_2H_2 is particularly noteworthy because $C_2H_2^{2+}$ serves as an ideal model for studying ultrafast proton separation,[12] molecular isomerization,[13,14] and reaction processes such as H_2^+ generation.[15,16] Previous studies have observed four dissociation channels of C_2H_2.[17] Of these, the channel resulting in $C^+ + CH_2^+$, which involves a proton-transfer isomerization process,[18–20] has attracted significant attention.

The KER spectrum is a powerful experimental tool for probing the initial and final states of dissociation products.[21–24] The population of the initial states of parent ions is influenced by parameters such as the type, velocity and charge state of the incident particles;[25–29] consequently, KER distributions provide a window into the fragmentation dynamics of molecular ions under varied experimental conditions. For example, in a 38 eV XUV pump–probe experiment, this isomerization occurs on the low-lying excited state $A^2\Sigma_g^+$ of the $C_2H_2^+$ ion, with a KER range of 5.8 eV $<$ KER $<$ 8 eV and a time scale of 52 ± 15 fs.[19] Building on this, Jiang *et al.*[17] also studied the two-body dissociation channels of $C_2H_2^{2+}$ by reacting XUV with C_2H_2 molecules. Through investigations of KER and fragment ion momentum distributions, they identified possible intermediate states in the stepwise dissociation process. In a complementary study, Gong *et al.*[30] investigated the proton transfer channel $C^+ + CH_2^+$ using a 400 nm intense femtosecond laser field. By analyzing the photoelectron energy spectra and angular distributions corresponding to different KER values, they found that electrons

†Corresponding author. E-mail: leijianting@hit.edu.cn
‡Corresponding author. E-mail: qingcao.liu@hit.edu.cn
§Corresponding author. E-mail: zhangshf@impcas.ac.cn

© 2026 Chinese Physical Society and IOP Publishing Ltd. All rights, including for text and data mining, AI training, and similar technologies, are reserved.

associated with the low-energy proton transfer channel were emitted via non-sequential double ionization from the C_2H_2 molecule. This process directly populates highly excited states of $C_2H_2^{2+}$, leading to proton transfer occurring in the $^3\Pi$ state of the dication. Moreover, Jochim *et al.*[31] combined potential energy curves corresponding to the C–C stretch of linear $C_2H_2^{2+}$ with the KER distribution of the symmetric channel measured under a strong field. They determined that the measured KER of 5 eV is related to dissociation over the potential barrier involving the $^1\Sigma_g^-$ state.

Although the fragmentation processes of symmetric molecules like C_2H_2 have been extensively studied, a key complexity arises because various electronic states of $C_2H_2^{2+}$ are populated in double ionization experiments — whether induced by electrons,[32–34] ions,[15,35,36] or strong laser fields.[30] The KER spectrum often incorporates contributions from dissociations of all electronic states, complicating the mechanistic interpretation of KER peaks. This challenge of state assignment is illustrated by several channels. In the $H^+ + C_2H^+$ channel, two peaks are observed in the KER distribution: a low-energy peak at 3.76 eV; the lowest electronic states $^3\Sigma_g^-$ and $^1\Sigma_g^-$ have energies of 3.5 eV and 3.6 eV, respectively. In the $CH_2^+ + C^+$ channel, a KER peak at 4.6 eV is found, whereas the lowest electronic states $^1\Delta_g$ and $^3\Sigma_g^-$ have energies of 4.5 eV and 4.0 eV, respectively, making it difficult to determine which electronic state dominates based on KER alone. Given the challenges in assigning electronic states solely based on KER spectra, analyzing the relative branching ratios of the major dissociation products, in conjunction with theoretical calculations, provides a more robust approach for distinguishing and elucidating the dominant dissociation mechanisms and pathways.

In this study, we investigated the dissociation processes of C_2H_2 molecules under 790 nm strong fields and electron collisions using a multiparticle coincidence momentum spectrometer. We obtained the KER and momentum distributions of ion fragments produced in the two-body dissociation of $C_2H_2^{2+}$ and the $(C_2H_2)_2$ dimer. By comparing the relative branching ratios at different laser power densities with *ab initio* and Rice–Ramsperger–Kassel–Marcus (RRKM) theoretical calculations, we found that the doubly ionized C_2H_2 dissociates primarily on the singlet ground-state potential energy surface under strong laser fields, whereas dissociation proceeds predominantly via the triplet ground state following electron impact. This work provides a straightforward method for studying C_2H_2 dissociation by comparing experimental branching ratios with theory, offering new insights into its behavior in strong laser fields.

2. Experimental methods

The experiment was conducted using a reaction microscope combined with a pulsed electron source and a Ti:sapphire laser system. The laser delivered pulses centered at 790 nm with a duration of 35 fs and a repetition rate of 3 kHz, producing peak intensities up to 9×10^{13} W/cm^2 at the interaction region. The target gas was prepared via supersonic expansion of helium seeded with C_2H_2 at 1 bar backing pressure through a 30 μm nozzle, followed by a two-stage differential pumping system, resulting in a cold molecular beam within a background vacuum maintained at 10^{-10} mbar. Fragment ions generated in the laser–molecule interaction were extracted and guided by a uniform electric field of 50 V/cm, then detected by a position- and time-sensitive microchannel plate detector equipped with a hexagonal delay-line readout. Time-of-flight and spatial information were recorded to reconstruct the full three-dimensional momentum vectors of the charged fragments. Additionally, a pulsed photoelectron emission gun intersected the molecular beam in the reaction zone, enabling 1 keV electron-impact ionization. Resulting fragment ions were analyzed by a time-of-flight mass spectrometer coupled to a two-dimensional time- and position-sensitive detector, facilitating coincident detection and momentum-resolved studies of electron–molecule collision dynamics.

3. Results and discussion

The TOF correlation map of C_2H_2 ionic fragments in an intense 790 nm laser field is presented in Fig. 1(a). For each dissociative channel, momentum-conserved correlated events form a distinct island on the map. Four correlation islands are identified, namely (a) $C_2H^+ + H^+$; (b) $CH_2^+ + C^+/CH^+ + CH^+$; (c) $C_2H_2^{2+} + C_2H_2^+$; and (d) $C_2H_2^+ + C_2H_2^+$. By employing tail-morphology analysis, the $C_2H^+ + H^+$ channel shows an asymmetrical long tail feature, which is primarily due to delayed dissociation from a metastable dication (highly vibrationally excited states of the electronic states $^3\Sigma_g^-$, $^1\Sigma_g^+$, and $^1\Delta_g$).[24] Due to the overlap between the $CH^+ + CH^+$ and $CH_2^+ + C^+$ channels in the TOF coincidence spectrum, which makes them indistinguishable as shown in Fig. 1(b), we employed a method based on the fact that the KER is independent of the dissociation angle to distinguish between the two channels. Channels (c) and (d) represent two distinct dissociation channels of the $(C_2H_2)_2$ dimer, respectively. In the following sections, these five dissociation channels will be discussed in detail.

For the channel $H^+ + C_2H^+$, the KER distribution measured in this experiment is shown in Fig. 2(a). The main peak of the KER is located around 3.76 eV, with a minor tailing peak observed at approximately 5 eV. According to the theoretically calculated potential energy curves shown in Fig. 2(b),

the higher-energy KER peak is mainly attributed to dissociation along the C–H bond on the excited electronic states $^3\Pi_u$ and $^1\Pi_u$, while the lower-energy peak arises from dissociation via highly vibrationally excited states of the electronic states $^3\Sigma_g^-$, $^1\Sigma_g^+$, and $^1\Delta_g$. In previous studies, Jiang *et al.*[19] investigated the deprotonation channel using 38 eV XUV photons and reported a KER distribution ranging from 3 eV to 8 eV, with the main peak centered at 5.2 ± 0.1 eV. Subsequently, in another study using 42 eV photons, single-photon double ionization of C_2H_2 revealed a bimodal KER distribution, with a dominant peak at 4.75 eV and a secondary peak at 3.75 eV. Similarly, Chen *et al.*[32] directly measured the KER distribution of this channel and found a major peak at 4.8 eV and a slight shoulder around 3.6 eV by electron impact at 1 keV. In strong-field ionization, the main KER peak is observed at 3.76 eV. However, when XUV photons or electrons are used as projectiles, the dominant peak shifts to 4.8 eV, highlighting a clear difference in the branching ratios within the KER distribution compared with strong-field ionization. This discrepancy can be attributed to the fact that strong laser fields may suppress the potential energy surface of the $^3\Sigma_g^-$ state, thereby facilitating dissociation.

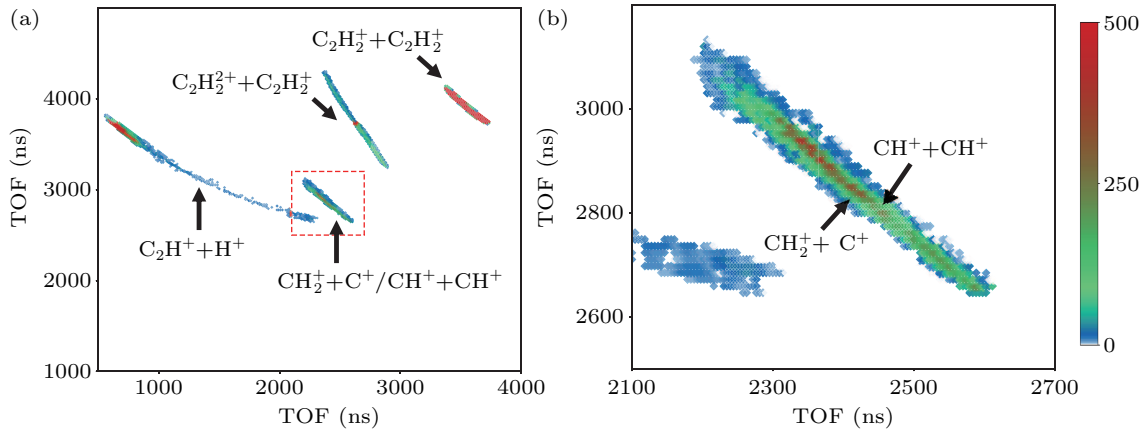


Fig. 1. Time-of-flight (TOF) correlation maps of ionic fragments from C_2H_2 in an intense 790 nm laser field. (a) The full TOF correlation map with multiple dissociation channels. (b) The magnified TOF correlation view of the C–C bond cleavage channels indicated by the red box in (a), corresponding to the $CH_2^+ + C^+$ and $CH^+ + CH^+$ dissociation pathways.

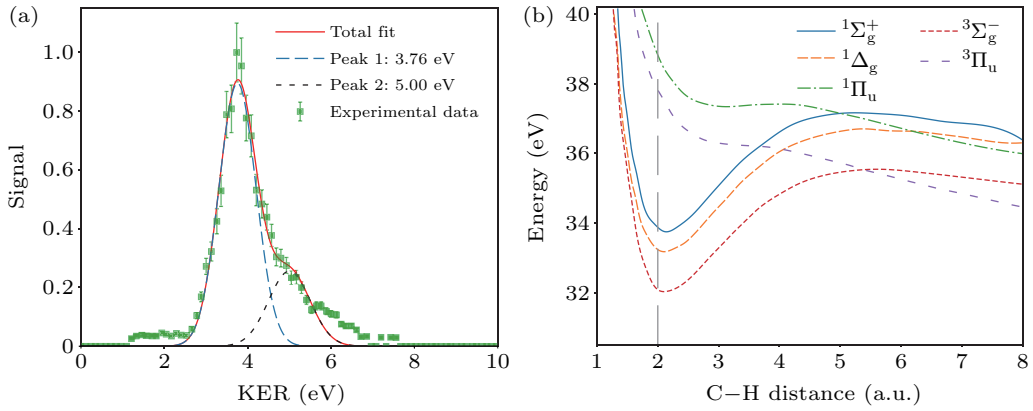


Fig. 2. (a) KER distribution for the $H^+ + C_2H^+$ dissociation channel measured under an intense laser field. (b) Calculated potential energy curves of $C_2H_2^{2+}$ along the C–H stretching coordinate, adapted from Gaire *et al.*,[35] illustrating the electronic states involved in the dissociation process.

To distinguish between the $CH^+ + CH^+$ and $C^+ + CH_2^+$ channels under an intense laser field, we employed a KER–θ analysis method to separate them. By selecting all events within correlation island b from the two-dimensional TOF spectrum, and respectively assuming that island b originates entirely from the dissociation channels of $CH^+ + CH^+$ or $C^+ + CH_2^+$, we constructed two KER–θ distributions, where θ is the angle between the outgoing ion and the direction of the electric field, as shown in Figs. 3(a) and 3(b). It is noteworthy that the vertical streak observed near ~ 5.0 eV in Fig. 3(a) corresponds to real $CH^+ + H^+$ dissociation events, correctly analyzed using their own mass pair. The accompanying tilted streaks, however, are projection artifacts. These artifacts arise because data belonging to the $C^+ + CH_2^+$ channel were inadvertently analyzed using the mass pair of the $CH^+ + CH^+$ channel. The vertical lines at KER = 5 eV and KER = 4.6 eV can be clearly distinguished, as indicated by the red dashed lines in Figs. 3(a) and 3(b). These respectively correspond to the real events from the channels $CH^+ + CH^+$ and $C^+ + CH_2^+$. The analysis ranges for the KER curves are determined by the reported KER peak values of different channels. The integral range of the angles is set from 160° to 180° for a better signal-

to-noise ratio.[35–39] Using this selected dataset, we obtained the accurate KER distributions of these two channels as presented in Figs. 3(c) and 3(d). For the $CH^+ + CH^+$ channel in Fig. 3(c), a clear peak is observed at 5.0 eV, along with a pronounced shoulder structure near 6.0 eV. Similar KER distributions for this channel have been reported in measurements using XUV photons,[35,37] electrons,[38] and highly charged ion collisions,[36,39] all revealing a KER peak around 5.0 eV, which is consistent with our experimental results. Gaire *et al.*[35] conducted theoretical investigations of this channel and showed that the KER feature around 5.0 eV primarily arises from dissociation of the molecule in highly vibrationally excited states of the low-lying electronic states $^3\Sigma_g^-$, $^1\Delta_g$ and $^1\Sigma_g^+$. In contrast, the 6.0 eV peak is likely attributed to the $^3\Pi_u$, $^1\Pi_u$ and $^3\Pi_g$ states, which undergo nonadiabatic crossings with the $^1\Sigma_u^-$, $^3\Sigma_u^+$ and $^3\Delta_u$ states, resulting in dissociation from these latter states. For the $C^+ + CH_2^+$ channel, the KER distribution exhibits a main peak at 4.6 eV. This channel involves isomerization, a process that has attracted considerable research interest. In the XUV experiment of this channel, two KER peaks, 4.8 ± 0.1 eV and 5.8 ± 0.1 eV, were found.[19] In another study using XUV light, a KER peak at 4.5 eV was observed and attributed mainly to the dissociation of $C_2H_2^{2+}$ ions in the excited states $^1\Delta_g$ and $^3\Sigma_g^-$.[35] According to the theoretical study of the isomerization dissociation pathway of the lowest electronic states $^1\Delta_g$ and $^3\Sigma_g^-$ in $C_2H_2^{2+}$, the peak KERs for dissociation of the above two electronic states were found to be 4.5 eV and 4.0 eV, respectively, which are consistent with the main KER peak at 4.6 eV in this experiment.

Using the same method, we obtained the KER distributions of the $CH^+ + CH^+$ and $C^+ + CH_2^+$ dissociation channels under 1 keV electron collisions, as shown in Fig. 3(d). For the $CH^+ + CH^+$ channel, compared with the KER distribution measured in strong laser fields, a pronounced shoulder appears near 8.0 eV. Based on calculations in Ref. [35], this broad structural feature arises from the dissociation of three highly excited states — $^1\Sigma_u^-$, $^3\Sigma_u^+$, and $^3\Delta_u$. For the $C^+ + CH_2^+$ channel, a low-energy KER peak at 4.5 eV and a broad feature around 6.0 eV are observed. Zhang *et al.*[36] attributed the low-energy peak to two low-lying excited states of $C_2H_2^{2+}$, namely $^1\Delta_g$ and $^3\Sigma_g^-$, while the broad feature at 6.0 eV was assigned to the higher excited state $^3\Pi_u$. When comparing the KER distributions obtained from strong laser fields and high-energy electron collision measurements, the dissociation of $C_2H_2^{2+}$ exhibits higher KER peaks under electron impact. This is because electrons can readily remove inner-shell electrons of C_2H_2, thereby ionizing the molecule to highly excited states.

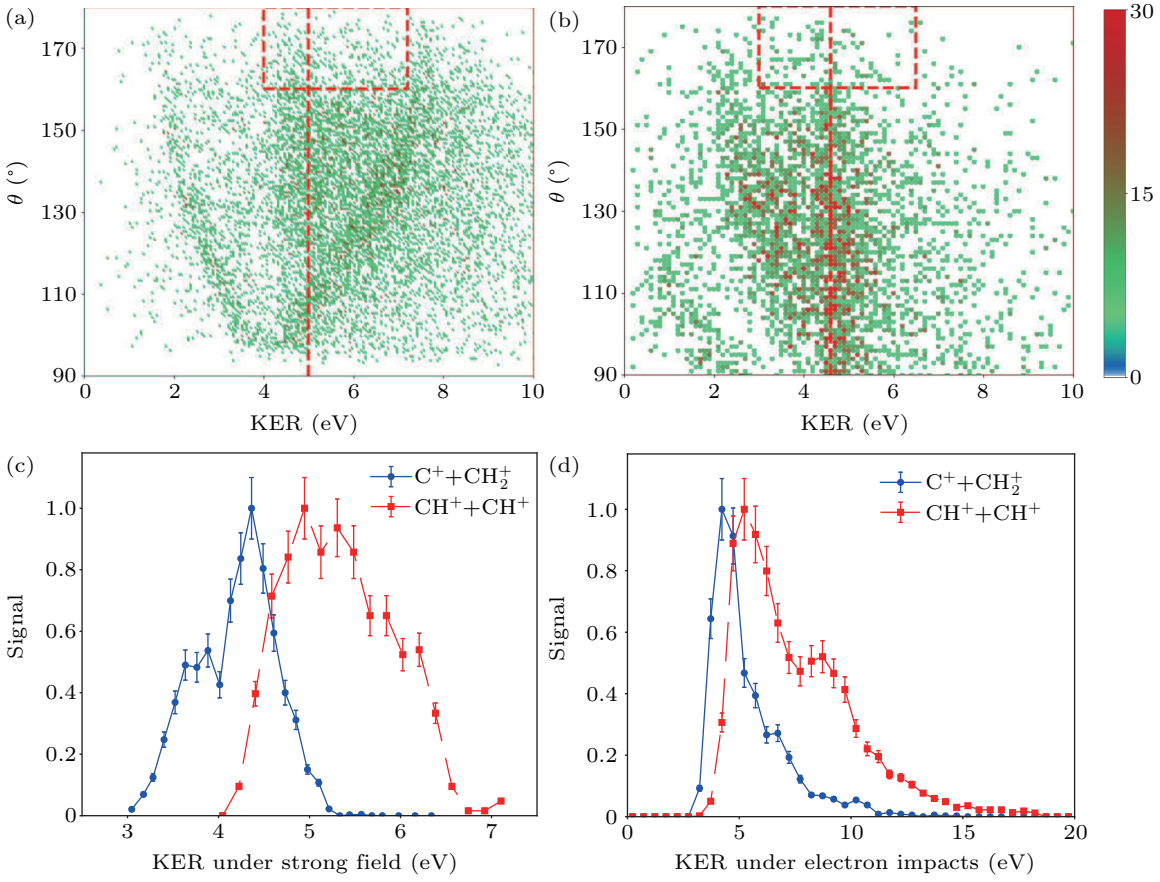


Fig. 3. KER distributions as a function of the dissociation angle θ for the (a) $C_2H_2^{2+} \rightarrow CH^+ + CH^+$ and (b) $C_2H_2^{2+} \rightarrow C^+ + CH_2^+$ channels under an intense laser field. The red dashed lines highlight the distinct KER values for each channel. (c) KER distributions for the $CH^+ + CH^+$ and $C^+ + CH_2^+$ channels, obtained by selecting events within the angular range of 160° to 180° (red dashed boxes in panels (a) and (b)) under laser irradiation. (d) Corresponding KER distributions for the same channels under 1 keV electron impact.

Figure 4 illustrates the branching ratios of the dissociation pathways of $C_2H_2^{2+}$ under electron impact as a function of incident electron energy ranging from 45 eV to 1000 eV. The branching ratio of the deprotonation channel decreases from 70% to 63% as the electron energy increases, while the $CH^+ + CH^+$ channel increases from 27% to 36%, with the $CH_2^+ + C^+$ channel remaining below 3%. Overall, the $C_2H^+ + H^+$ channel dominates at lower energies, whereas the $CH^+ + CH^+$ channel becomes more prominent with increasing energy, and the $C^+ + CH_2^+$ pathway remains minor.

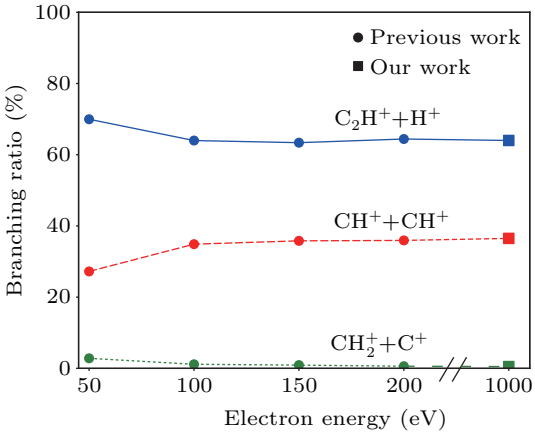


Fig. 4. Branching ratios of the charge-separating dissociation channels of $C_2H_2^{2+}$ as a function of the ionizing electron energy. The first four data points (electron energies ~50–200 eV) are adapted from Ref. [34].

In contrast to electron-impact ionization, Table 1 summarizes the relative branching ratios of the three dissociation channels under strong-field laser conditions and compares them with prior studies performed at different wavelengths and power densities. In the current experiment, the deprotonation channel dominates (57%), while the $CH^+ + CH^+$ and $C^+ + CH_2^+$ channels account for 18% and 25%, respectively. At a wavelength of 395 nm, as the power density increases from 3.6×10^{14} W/cm^2 to 6×10^{14} W/cm^2, the ratio of $CH^+ + CH^+$ to $C^+ + CH_2^+$ changes from 5:2 to 4:1, indicating a corresponding increase in the relative yield of $CH^+ + CH^+$ products along with a noticeable decrease in the isomerization channel $C^+ + CH_2^+$. At 790 nm, increasing the power density from 9×10^{13} W/cm^2 to 2×10^{14} W/cm^2 shifts the product branching ratio between the $CH^+ + CH^+$ and $C^+ + CH_2^+$ channels from 18:25 to 19:23, indicating a slight increase in the relative abundance of the former channel, accompanied by a corresponding decrease in the latter. This trend continues toward higher intensities: as the power density is further increased to 5×10^{15} W/cm^2, the ratio shifts toward 1:1, making the yields of the two channels comparable at high intensity. Notably, a comparison across wavelengths reveals that the yield ratio of $CH^+ + CH^+$ to $C^+ + CH_2^+$ is significantly lower under 790 nm irradiation than at 395 nm, implying a substantially greater relative yield of the isomerization channel at the longer wavelength. This notable yield of the isomerization channel under laser excitation stands in sharp contrast to its minor role (< 3% branching ratio) in electron-impact ionization. This highlights the distinct dissociation mechanisms between coherent laser excitation and statistical electron-impact processes, leading to markedly different product branching ratios. Overall, it is demonstrated that the wavelength (photon energy) and power density collaboratively regulate the double-ionization dissociation pathways of C_2H_2, thereby influencing the product distribution.

Table 1. Ratios of $(CH^+ + CH^+)$ to $(CH_2^+ + C^+)$ as a function of wavelength and power density.

λ (nm)	P (w/cm^2)	$(CH^+ + CH^+)$:$(CH_2^+ + C^+)$
395[a]	3.6×10^{14}	5:2
395[b]	6×10^{14}	4:1
790	9×10^{13}	18:25
790[c]	2×10^{14}	19:23
790[b]	5×10^{15}	1:1

[a]Ref. [20], [b]Ref. [31], [c]Ref. [30].

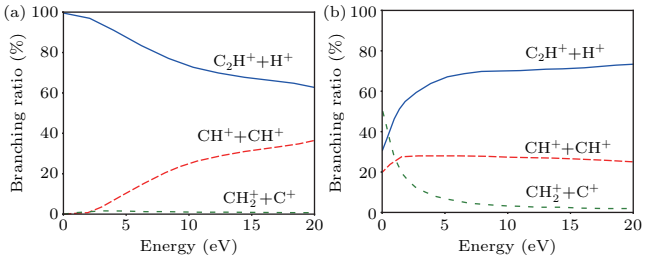


Fig. 5. Calculated branching ratios of various fragmentation channels of $C_2H_2^{2+}$ as a function of the internal energy if dissociation occurs on the (a) ground triplet and (b) lowest singlet potential energy surfaces, reproduced from Zyubina *et al.*[40] with permission.

Zyubina *et al.*[40] investigated the dissociation mechanisms of C_2H_2 on the ground triplet state ($^3\Sigma_g^-$), singlet state ($^1\Delta_g$), and excited states using high-level quantum chemical calculations and RRKM kinetic theory. As illustrated in Fig. 5(a), their theoretical predictions indicate that if dissociation occurs exclusively on the triplet-state ($^3\Sigma_g^-$) potential energy surface, the branching ratio of the deprotonation channel decreases from 100% to 62% as internal energy increases, while the $CH^+ + CH^+$ channel increases from 0.2% to 37%, with the $CH_2^+ + C^+$ channel remaining below 2%. In contrast, Fig. 5(b) shows that on the singlet ground-state ($^1\Delta_g$) potential energy surface, the branching ratio for the $CH_2^+ + C^+$ channel starts from a maximum of 50% but drops rapidly to below 3% at higher energies. The deprotonation branching ratio rises sharply from 30% to over 65% as internal energy increases from 4.2 eV to 8 eV, while the $CH^+ + CH^+$ channel stabilizes at around 26% for internal energies above 5 eV. Under electron-impact conditions, considering the dissociation energy and energy transfer efficiency,[35] it can be estimated that as the internal energy of $C_2H_2^{2+}$ increases from 3 eV to 20 eV, dissociation predominantly aligns with the ground triplet surface. This suggests that under electron-impact ionization, the

dissociation of $C_2H_2^{2+}$ primarily occurs on the ground triplet-state potential energy surface. Similarly, as shown in Table 1, under various experimental laser conditions, the internal energy of $C_2H_2^{2+}$ is estimated to fall within the range of 3–10 eV. Across these intensities, the branching ratio of the $CH_2^+ + C^+$ channel remains significant, which is inconsistent with the predictions for the ground triplet surface, but aligns well with those for the ground singlet surface. This indicates that strong-field laser-induced dissociation of $C_2H_2^{2+}$ primarily proceeds on the ground singlet-state potential energy surface. In contrast, the differing branching ratios observed between strong-field laser and electron-collision experiments arise because dissociation predominantly occurs via the singlet ($^1\Delta_g$) and triplet ($^3\Sigma_g^-$) states, respectively. For electron collisions, the preference for the triplet state aligns with the propensity rule (valence-bond framework), which favors the triplet state due to its lower potential energy surface. This rule implies that near-threshold electron-impact double ionization tends to favor triplet over singlet pathways. When the laser field is aligned with either of the π orbitals, the two electrons residing in that particular orbital are preferentially ionized, and due to the Pauli exclusion principle, the resulting state is a singlet ground state.

Figure 6(a) shows the KER distribution for $(C_2H_2)_2^{2+} \rightarrow C_2H_2^+ + C_2H_2^+$, with a peak at 3.05 eV. According to KER = 14.4 (Q_1Q_2/R), dissociation occurs at a nuclear distance of 4.72 Å. Xu *et al.*[41] studied the divalent symmetric dissociation of $(C_2H_2)_2^{2+}$ using 200 keV He^{2+} ions and obtained a molecular spacing of 4.4 Å through KER. Reference [42] shows the KER distribution calculated by molecular dynamics simulation, with a peak value of approximately 3.18 eV, which is similar to the experimental KER. The slight deviation in the peak value may be due to the deformation of the dimer structure caused by the strong laser field in the experiment. As shown in Fig. 6(b), through the two-dimensional momentum distribution of $C_2H_2^+$ in the laser plane, it was found that $C_2H_2^+$ ions exhibit anisotropy and mainly exit along the laser polarization direction (x), indicating that the dissociation time of $(C_2H_2)_2$ dications is faster than the rotation period of $(C_2H_2)_2$.

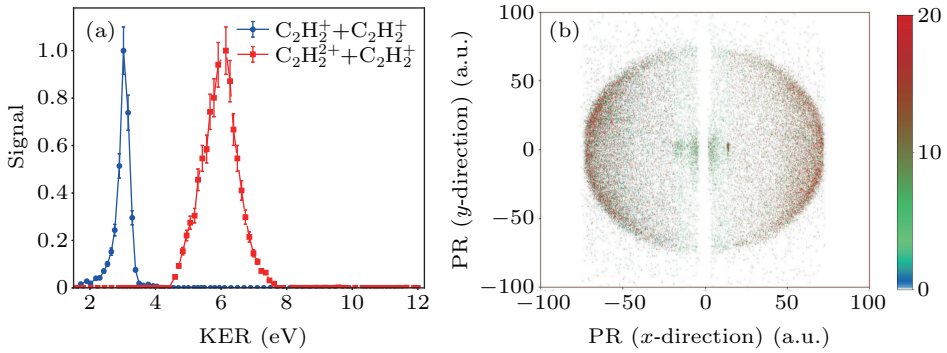


Fig. 6. (a) KER distributions under laser irradiation for the dimer dissociation channels $(C_2H_2)_2^{2+} \rightarrow C_2H_2^+ + C_2H_2^+$ and $(C_2H_2)_2^{2+} \rightarrow C_2H_2^{2+} + C_2H_2^+$. (b) Two-dimensional momentum distribution of $C_2H_2^+$ fragments in the laser polarization plane for the $(C_2H_2)_2^{2+} \rightarrow C_2H_2^+ + C_2H_2^+$ channel, showing anisotropic emission along the laser polarization direction (x-axis).

For the $(C_2H_2)_2^{3+} \rightarrow C_2H_2^{2+} + C_2H_2^+$ dissociation channel, Fig. 6(a) shows that the experimentally measured KER values exhibit a unimodal structure, with a peak at 6.1 eV. This result can be interpreted as a direct transition of $(C_2H_2)_2$ from the neutral ground state to the repulsive state $C_2H_2^+$–$C_2H_2^{2+}$ under the induction of laser pulses. Using the point-charge approximation, the instantaneous molecular spacing of $(C_2H_2)_2^{3+}$ Coulomb explosion is approximately 4.72 Å, consistent with that of $(C_2H_2)_2^{2+}$ dissociation. These results indicate that $(C_2H_2)_2^{2+}$ and $(C_2H_2)_2^{3+}$ follow similar physical processes on the same timescale under strong-field-induced dissociation. Specifically, following the single ionization of one neutral C_2H_2 molecule within the dimer, the liberated electron is driven by the strong laser field to recollide with the parent $(C_2H_2)_2^+$ ion. This recollision induces non-sequential double ionization of the second C_2H_2 molecule, ultimately leading to the Coulomb explosion of the trication $(C_2H_2)_2^{3+}$.

4. Conclusion

This study investigates the two-body dissociation and fragmentation mechanisms of $C_2H_2^{2+}$ under strong laser fields and electron impact. All dissociation channels of $C_2H_2^{2+}$, as well as those of $(C_2H_2)_2^{2+}$, were identified, and the corresponding time-of-flight spectra and KER distributions were obtained. Particular emphasis was placed on analyzing the three main dissociation channels of $C_2H_2^{2+}$ — $C_2H^+ + H^+$, $CH_2^+ + C^+$, and $CH^+ + CH^+$ — by examining the trends in their branching ratios to determine the contributions of the dissociative states. The deprotonation channel $H^+ + C_2H^+$ shows peaks at 3.76 eV and 5.0 eV; the symmetric $CH^+ + CH^+$ channel peaks at 5.0 eV with a 6.0 eV shoulder; and the isomerization channel $C^+ + CH_2^+$ peaks at 4.6 eV. These features reflect contributions from both ground and excited electronic states, but the dissociation is predominantly governed by the ground-state potential energy surfaces. Comparison of KER

distributions obtained under strong-field laser ionization and 1 keV electron-impact ionization reveals that $C_2H_2^{2+}$ exhibits a higher KER peak under electron impact, primarily due to high-energy electrons ionizing inner-shell electrons of C_2H_2, promoting the molecule to highly excited states. Furthermore, analysis of the branching ratios indicates that strong-field laser-induced dissociation predominantly occurs along the singlet $^1\Delta_g$ potential energy surface, whereas electron-impact-induced dissociation proceeds mainly via the triplet $^3\Sigma_g^-$ surface, underscoring the decisive influence of excitation conditions on the dissociation pathways. This distinction fundamentally arises from the coupling between molecular orbital orientation and the laser field. In addition, for $(C_2H_2)_2$, both $(C_2H_2)_2^{2+}$ and $(C_2H_2)_2^{3+}$ dissociate at 4.72 Å, consistent with Coulomb explosion. Overall, these results provide new insights into the dissociation dynamics of C_2H_2 under distinct ionization regimes.

Acknowledgments

This work was supported by the National Natural Science Foundation of China (Grant Nos. 12304376, 12504397, and 12204132), the Shandong Provincial Natural Science Foundation (Grant Nos. ZR2025QC1459, ZR2025QC1458, tsqn202408113, and ZR2023QA075), and the National Key Research and Development Program of China (Grant No. 2022YFA1602500).

References

[1] Zhao L, Kaiser R I, Xu B, Ablikim U, Ahmed M, Evseev M M, Bashkirov E K, Azyazov V N and Mebel A M 2018 *Nat. Astron.* **2** 973
[2] Joblin C and Tielens A G G M 2020 *PAHs and the Universe* (EDP Sciences)
[3] Lemmens A K, Rap D B, Thunnissen J M M, Willemsen B and Rijs A M 2020 *Nat. Commun.* **11** 269
[4] Parker D S N, Kaiser R I, Kostko O, Troy T P, Ahmed M, Sun B J, Chen S H and Chang A H H 2015 *Phys. Chem. Chem. Phys.* **17** 32000
[5] Levey Z D, Laws B A, Sundar S P, Nauta K, Kable S H, Da Silva G, Stanton J F and Schmidt T W 2022 *J. Phys. Chem. A* **126** 101
[6] Hudson R, De Graaf R, Strandoo Rodin M, Ohno A, Lane N, McGlynn S E, Yamada Y M A, Nakamura R, Barge L M, Braun D and Sojo V 2020 *Proc. Natl. Acad. Sci. USA* **117** 22873
[7] Cho Y S, Oh I H, Kim J H, Kim J I, Lee K B and Nah I W 2025 *Sci. Rep.* **15** 2085
[8] Ruiz-Mirazo K, Briones C and De La Escosura A 2017 *Open Biol.* **7** 170050
[9] Bai Y, Fu Y L, Qi J, Liu L, Lu X, Han Y C, Zhang D H and Fu B 2025 *Nat. Commun.* **16** 2732
[10] Taylor S S, Varga K, Mogyorósi K, Chikán V and Covington C 2025 *Phys. Rev. A* **111** 013109
[11] Lee Y C, Venkatesan V, Lee Y P, Macko P, Didiriche K and Herman M 2007 *Chem. Phys. Lett.* **435** 247
[12] Luzon I, Livshits E, Gope K, Baer R and Strasser D 2019 *J. Phys. Chem. Lett.* **10** 1361
[13] Li Z, Inhester L, Liekhus-Schmaltz C, Curchod B F E, Snyder J W, Medvedev N, Cryan J, Osipov T, Pabst S, Vendrell O, Bucksbaum P and Martinez T J 2017 *Nat. Commun.* **8** 453
[14] Xu S, Zhao H, Zhu X, Guo D, Feng W, Lau K C and Ma X 2018 *Phys. Chem. Chem. Phys.* **20** 27725
[15] Saito N, Nagoshi M, Machida M, Koyano I, De Fanis A and Ueda K 2004 *Chem. Phys. Lett.* **393** 295
[16] Laksman J, Céolin D, Gisselbrecht M, Canton S E and Sorensen S L 2009 *J. Chem. Phys.* **131** 244305
[17] Jiang Y H, Senftleben A, Kurka M, Rudenko A, Foucar L, Herrwerth O, Kling M F, Lezius M, Tilborg J V, Belkacem A, Ueda K, Rolles D, Treusch R, Zhang Y Z, Liu Y F, Schröter C D, Ullrich J and Moshammer R 2013 *J. Phys. B* **46** 164027
[18] Wells E, Rallis C E, Zohrabi M, Siemering R, Jochim B, Andrews P R, Ablikim U, Gaire B, De S, Carnes K D, Bergues B, De Vivie-Riedle R, Kling M F and Ben-Itzhak I 2013 *Nat. Commun.* **4** 2895
[19] Jiang Y H, Rudenko A, Herrwerth O, Foucar L, Kurka M, Kühnel K U, Lezius M, Kling M F, Van Tilborg J, Belkacem A, Ueda K, Düsterer S, Treusch R, Schröter C D, Moshammer R and Ullrich J 2010 *Phys. Rev. Lett.* **105** 263002
[20] Gong X, Song Q, Ji Q, Lin K, Pan H, Ding J, Zeng H and Wu J 2015 *Phys. Rev. Lett.* **114** 163001
[21] Dujardin G, Winkoun D and Leach S 1985 *Phys. Rev. A* **31** 3027
[22] Das R, Pandey D K, Soumyashree S, Madhusudhan P, Nimma V, Bhardwaj P, Shameem K M M, Singh D K and Kushawaha R K 2022 *Phys. Chem. Chem. Phys.* **24** 18306
[23] Kinugawa T, Lablanquie P, Penent F, Palaudoux J and Eland J H D 2004 *J. Electron Spectrosc. Relat. Phenom.* **141** 143
[24] Larimian S, Erattupuzha S, Lötstedt E, Szidarovszky T, Maurer R, Roither S, Schöffler M, Kartashov D, Baltuška A, Yamanouchi K, Kitzler M and Xie X 2016 *Phys. Rev. A* **93** 053405
[25] Shi G, Xiang Y, Lei J, Sun S, Liu Z and Hu B 2023 *Eur. Phys. J. D* **77** 20
[26] Lv H, Zuo W, Zhao L, Xu H, Jin M, Ding D, Hu S and Chen J 2016 *Phys. Rev. A* **93** 033415
[27] Liu Y, Yi X, Chen Q, Sun T, Lv H, Hu S, Becker W, Xu H and Chen J 2024 *Photonics Res.* **12** 3033
[28] Zhang B, Chen W and Zhao Z 2014 *Phys. Rev. A* **90** 023409
[29] Sun R and Xin P 2024 *Phys. Scr.* **99** 105412
[30] Gong X, Song Q, Ji Q, Pan H, Ding J, Wu J and Zeng H 2014 *Phys. Rev. Lett.* **112** 243001
[31] Jochim B, Zohrabi M, Severt T, Berry B, Betsch K J, Feizollah P, Rajput J, Wells E, Carnes K D and Ben-Itzhak I 2020 *Phys. Rev. A* **101** 013406
[32] Chen L, Shan X, Wang E L, Ren X G, Zhao X, Huang W Z and Chen X J 2019 *Phys. Rev. A* **100** 062707
[33] Xie X, Roither S, Schöffler M, Lötstedt E, Kartashov D, Zhang L, Paulus G G, Iwasaki A, Baltuška A, Yamanouchi K and Kitzler M 2014 *Phys. Rev. X* **4** 021005
[34] King S J and Price S D 2007 *J. Chem. Phys.* **127** 174307
[35] Gaire B, Lee S Y, Haxton D J, Pelz P M, Bocharova I, Sturm F P, Gehrken N, Honig M, Pitzer M, Metz D, Kim H-K, Schöffler M, Dörner R, Gassert H, Zeller S, Voigtsberger J, Cao W, Zohrabi M, Williams J, Gatton A, Reedy D, Nook C, Müller T, Landers A L, Cocke C L, Ben-Itzhak I, Jahnke T, Belkacem A and Weber Th 2014 *Phys. Rev. A* **89** 013403
[36] Zhang Y, Wang B, Wei L, Jiang T, Yu W, Hutton R, Zou Y, Chen L and Wei B 2019 *J. Chem. Phys.* **150** 204303
[37] Alagia M, Callegari C, Candori P, Falcinelli S, Pirani F, Richter R, Stranges S and Vecchiocattivi F 2012 *J. Chem. Phys.* **136** 204302
[38] Wang B, Wei L, Zhang Y, Yu W, Zou Y, Chen L and Wei B 2020 *J. Phys. B* **53** 155205
[39] De S, Rajput J, Roy A, Ghosh P N and Safvan C P 2008 *Phys. Rev. A* **77** 022708
[40] Zyubina T S, Dyakov Y A, Lin S H, Bandrauk A D and Mebel A M 2005 *J. Chem. Phys.* **123** 134320
[41] Xu S, Guo D, Ma X, Zhu X, Feng W, Yan S, Zhao D, Gao Y, Zhang S, Ren X, Zhao Y, Xu Z, Dorn A, Cederbaum L S and Kryzhevoi N V 2018 *Angew. Chem. Int. Ed.* **57** 17023
[42] Zhou J, He C, Liu M M, Wang E, Jia S, Dorn A, Ren X and Liu Y 2021 *Phys. Rev. Res.* **3** 023050